Influence of passive elements on the dynamics of oscillatory ensembles of cardiac cells

V. S. Petrov,[1,2] G. V. Osipov,[1,2] and J. A. K. Suykens[2]
[1]*Department of Control Theory, Nizhny Novgorod University, Gagarin Avenue 23, 603950 Nizhny Novgorod, Russia*
[2]*K. U. Leuven, ESAT-SCD/SISTA, Kasteelpark Arenberg 10, B-3001 Leuven (Heverlee), Belgium*
(Received 13 January 2009; published 29 April 2009)

In this paper we focus on the influence of passive elements on the collective dynamics of oscillatory ensembles. Two major effects considered are (i) the influence of passive elements on the synchronization properties of ensembles of coupled nonidentical oscillators and (ii) the influence of passive elements on the wave dynamics of such systems. For the first effect, it is demonstrated that the introduction of passive elements may lead to both an increase or decrease in the global synchronization threshold. For the second effect, it is also demonstrated that the steady state of the passive element is a key parameter which defines how this passive element affects the wave dynamics of the oscillatory ensemble. It was shown that for different values of this parameter, one can observe increase or decrease in wave propagation velocity and increase or decrease in synchronization frequency in oscillatory ensembles with the growth of influence of passive elements. The results are obtained for the models of cardiac cells dynamics as well as for the Bonhoeffer–Van der Pol model and are compared with data of real biological experiments.

DOI: 10.1103/PhysRevE.79.046219 PACS number(s): 05.45.Xt

I. INTRODUCTION

The study of collective dynamical effects in systems of coupled elements is one of the modern problems of many branches of physics [1–4]. Lately various kinds of collective behavior have been considered in systems with a nonhomogeneous distribution of parameters [5–7]. However, the presence of another type of inhomogeneity is characteristic for many real systems. In [8], for example, the role of heterogeneity in the emergence of global oscillations in the initially excitable medium was discussed. Such systems consist of elements having essentially different dynamics, namely, oscillatory and/or excitable and/or passive elements. In this way, for example, the heart may be considered as a dynamical system which is an ensemble consisting of such elements [9,10]. The heart tissue is composed of cells of three major types: pacemaker cells (pacemakers), cardiomyocytes, and fibroblasts that from the point of view of nonlinear dynamics are oscillatory, excitable, and passive elements, respectively. The main difference between these certain cell types is that pacemakers are able to generate periodic oscillations of electrical action potentials, while cardiomyocytes can only produce an action potential in response to the incoming stimulus. Fibroblasts, in turn, do not generate action potentials even in response to external excitation but just relax to the steady state.

In this paper, the emphasis is put on the interaction between oscillatory and passive elements. In the heart such kind of interaction is observed in the sinoatrial node that consists of pacemakers and fibroblasts. The amount of the latter cells in this region of the heart may come to 60–70 % according to the physiological experiments [11]. Apart from it, the total number of fibroblasts can vary in time due to the heart tissue aging processes or various kinds of diseases. The influence of these cells on the dynamics of the sinoatrial node and the heart in general is the subject of many studies based on biological experiments as well as numerical simulations [12–15]. In these papers, many evidences are presented indicating that the presence of fibroblasts may affect the synchronization properties of cells in the sinoatrial node, as well as deeply influence the characteristics of wave processes in the system, e.g., action potential conduction velocity. From the point of view of the heart functioning, this may lead to the development of different arrhythmias. Numerical simulations alongside with the use of nonlinear dynamics methods allow to explain the dynamical origin of such effects and it proposes various ways of controlling them. That is why the study of dynamics of mixed ensembles of oscillatory and passive elements is an important and acute task.

This paper is composed of two major parts. In the first part, the influence of passive elements on synchronization properties of oscillatory ensembles, namely, threshold and frequency of synchronization, is observed. First, the results of simulations with Bonhoeffer–Van der Pol oscillator (also known as FitzHugh-Nagumo system) are presented and an analytical description of the observed effects is given using the model of phase oscillators. Very often [8,16] cells of different types are described by phenomenological Bonhoeffer–Van der Pol model with different parameters. This is the simple but usually good enough approximation because it reproduces oscillatory, excitable, or passive dynamics depending on the value of parameters. This model also describes such characteristics of heart cells such as generation threshold, action potential, and others. Then we discuss results of simulations obtained using a biophysically relevant model of cardiac cells and compare these results with the data of real biological experiments.

In the second part of the paper, the influence of passive elements on the wave dynamics of oscillatory ensembles is discussed. Particularly, the accent is on the impact on the amplitude, frequency, and velocity of action potential propagation in the system of coupled cardiac cells. In this part of the paper, the results of numerical simulations are presented and compared with data of physiological research.

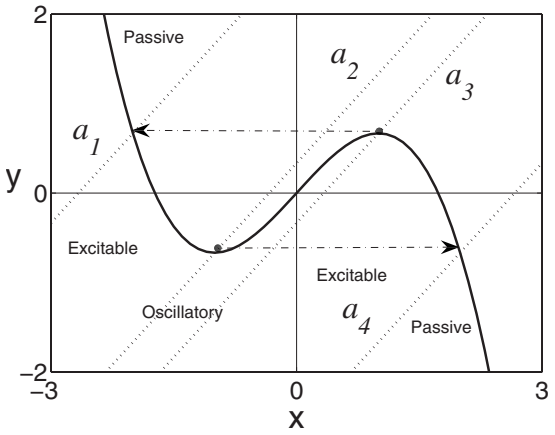

FIG. 1. Regions of oscillatory, excitable, and passive behavior of a Bonhoeffer–Van der Pol system. The solid line is the curve of slow motions. Dotted lines, dividing the areas of different system behavior, are nullclines of horizontal slopes for different values of control parameter $a_1=8/3$, $a_2=1/3$, $a_3=-1/3$, $a_4=-8/3$.

II. INFLUENCE OF PASSIVE ELEMENTS ON THE SYNCHRONIZATION PROPERTIES OF OSCILLATORY ENSEMBLES

A. Dynamical regimes in pair: Oscillatory element and passive element

In this section, the interaction between oscillatory and passive Bonhoeffer–Van der Pol elements is studied. Isolated oscillator is described by a system of two ordinary differential equations,

$$\dot{x} = x - x^3/3 - y,$$

$$\dot{y} = \varepsilon(x + a - y). \tag{1}$$

In application to biological systems, x in Eq. (1) denotes the action potential and y plays the role of the variables describing the ionic currents flowing through the membrane of a cell. The parameter a is the control parameter. By varying this parameter, one can observe different dynamical regimes of isolated elements: oscillatory, excitable, and passive [16]. This feature allows us to use this system as a simplified version of biological cell model applicable to study the main dynamical properties.

The curve of slow motions of the system (1) (nullcline: $y=x-x^3/3$) is shown as a solid line in Fig. 1. Nullclines of horizontal slopes $y=x+a$ for different values of a are plotted in Fig. 1 with dotted lines. For parameter range $(a<-8/3)\cup(a>8/3)$, the system is passive. When $-1/3<a<1/3$, the system is in oscillatory regime. For all other values of parameter a the system (1) exhibits excitable behavior.

Let us now consider a system consisting of two unidirectionally coupled oscillatory and passive elements,

$$\dot{x}_o = x_o - x_o^3/3 - y_o + d(x_o - x_p),$$

$$\dot{y}_o = \varepsilon(x_o + a_o - y_o),$$

$$\dot{x}_p = x_p - x_p^3/3 - y_p,$$

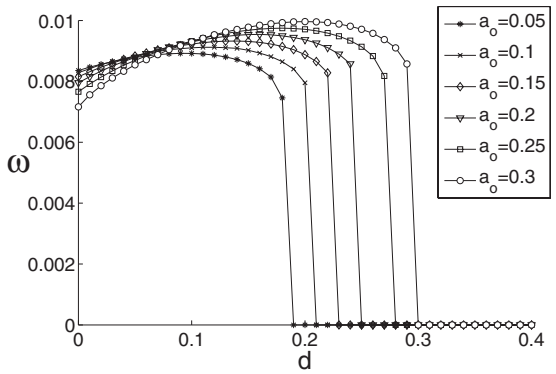

FIG. 2. Dependency of the oscillation frequency ω of the oscillatory Bonhoeffer–Van der Pol element on the parameter of the unidirectional coupling with a passive element d for different values of the parameter a_o. One can observe (i) a decrease in an effective frequency mismatch between elements with initially different individual frequencies caused by increasing the impact from the passive element till a certain critical value of d; (ii) an increase in the effective frequency mismatch between the elements; and (iii) vanishing of oscillations in the oscillatory element.

$$\dot{y}_p = \varepsilon(x_p + a_p - y_p). \tag{2}$$

The parameters a_o and a_p in Eq. (2) were chosen in such a way that the first and the second elements were in oscillatory and passive regimes, respectively. The individual frequency of the oscillatory element depends on value of a_o. The term $d(x_o-x_p)$ describes the unidirectional influence of the passive element on the oscillatory one.

Figure 2 illustrates the dependency of the oscillation frequency ω of the first Bonhoeffer–Van der Pol element on the parameter of unidirectional coupling with the passive element d for different values of parameter a_o corresponding to different individual frequencies of the oscillator.

It is clearly seen that every two curves in Fig. 2 have an intersection point. That means that for two oscillatory Bonhoeffer–Van der Pol elements with initially different individual frequencies, there exists such a coupling value d with the passive element, when the effective frequency mismatch will equal to zero. With the further growth of d, this effective frequency mismatch increases. Thus, the influence of a passive element changes the frequency of an oscillatory element and therefore affects the synchronization properties in such systems. Besides, it is worth saying that for some critical coupling value d in this system, the effect of oscillatory death is observed, i.e., vanishing of oscillations in the initially oscillatory element. In order to describe this effect, one can investigate the dependency of system (2) steady-state coordinates and their stability on the coupling parameter d. Supposing right-hand side parts of the system being zero, we can obtain the equation for the coordinate x_o of the steady state,

$$x_o^3 + 3dx_o + 3(a_o - dx_p^*) = 0, \tag{3}$$

where $x_p^*=\sqrt[3]{3a_p}$. Equation (3) has the only real root,

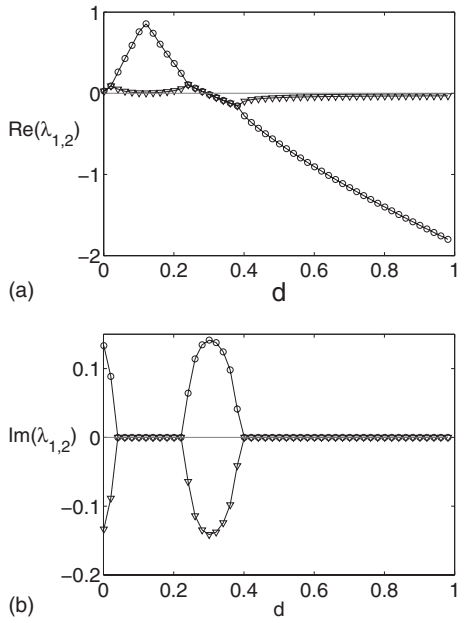

FIG. 3. (a) Real and (b) imaginary parts of the roots $\lambda_{1,2}$ of Eq. (5) depending on parameter d for fixed values $a_o=0.3$, $x_p^*=2.5$. Due to the subcritical Andronov-Hopf bifurcation the steady state of the system (2) acquires stability for $d\approx 0.29$.

$$x_o^* = \frac{1}{2}\sqrt[3]{\xi} - \frac{2d}{\sqrt[3]{\xi}}, \tag{4}$$

where

$$\xi = -12(a_o - dx_p^*) + 4\sqrt{4d^3 + 9(a_o - dx_p^*)^2}.$$

The stability of this steady state is defined by the roots $\lambda_{1,2}$ of the following characteristic equation:

$$\lambda^2 + \lambda(d + x_o^{*2} + \varepsilon - 1) + \varepsilon(d + x_o^{*2}) = 0. \tag{5}$$

Real and imaginary parts of the roots $\lambda_{1,2}$ of Eq. (5) depending on parameter d for fixed values $a_o=0.3$, $x_p^*=2.5$ are presented in Figs. 3(a) and 3(b), respectively. The figure shows that initially unstable focus $\{\mathrm{Re}(\lambda_{1,2})>0,\ \mathrm{Im}(\lambda_{1,2})\neq 0,\ d\in[0,0.041]\}$ with growth of d becomes at first an unstable node $\{\mathrm{Re}(\lambda_{1,2})>0,\ \mathrm{Im}(\lambda_{1,2})=0,\ d\in[0.041,0.22]\}$ and after that an unstable focus again. Then for $d\approx 0.29$ the real parts of the two complex-conjugate roots of the characteristic Eq. (5) get equal to zero and become negative with a further increase of d. Thereby, the steady state of system (2) acquires stability via an Andronov-Hopf bifurcation. A more detailed investigation shows that this bifurcation is subcritical and it is accompanied with the birth of an unstable limit cycle. Finally, for $d\approx 0.298$ the stable and unstable limit cycles merge and disappear via a saddle-node limit cycle bifurcation. After that, the oscillations in system (2) die out.

Apart from it, it is also worth saying that almost the opposite effect may take place in this system for other values of parameters. It was shown in [8] that introduction of diversity, i.e., parameter mismatch, in the initially homogeneous excitable medium of Bonhoeffer–Van der Pol elements leads to the emergence of global oscillations with the growth of coupling between oscillators.

B. Synchronization of two oscillatory Bonhoeffer–Van der Pol elements under the influence of a passive element

Let us now proceed to the study of the influence of a passive element on the threshold and frequency of synchronization. Consider the system of three coupled Bonhoeffer–Van der Pol elements,

$$\begin{aligned}
\dot{x}_{o1} &= x_{o1} - x_{o1}^3/3 - y_{o1} + d_1(x_{o2} - x_{o1}) + d_2(x_p - x_{o1}),\\
\dot{y}_{o1} &= \varepsilon(x_{o1} + a_{o1} - y_{o1}),\\
\dot{x}_{o2} &= x_{o2} - x_{o2}^3/3 - y_{o2} + d_1(x_{o1} - x_{o2}) + d_2(x_p - x_{o2}),\\
\dot{y}_{o2} &= \varepsilon(x_{o2} + a_{o2} - y_{o2}),\\
\dot{x}_p &= x_p - x_p^3/3 - y_p,\\
\dot{y}_p &= \varepsilon(x_p + a_p - y_p).
\end{aligned} \tag{6}$$

Let the first two elements be oscillatory with different individual frequencies. To be more concrete, let us consider $a_{o1}=0.31$ and $a_{o2}=0.25$. Coefficients d_1 and d_2 describe the interaction between the oscillatory elements and the unidirectional impact from the passive element on them, respectively. As far as in this situation the limit case of unidirectional coupling is observed, the passive element is in its steady state $x_p=x_p^*$. Parameter a_p was chosen in simulations such that $x_p^*=2.5$.

Figure 4(a) demonstrates the synchronization threshold d_1^s tuning coupling with passive element d_2. It is seen that with an increasing influence of the passive element on the oscillatory ones, a significant lowering of the synchronization threshold d_1^s takes place. At $d_1^s\approx 0.11$ it almost reaches zero. Then the value of the synchronization threshold starts to increase back again and, starting from a certain value of $d_2\approx 0.25$, even exceeds the initial value that was observed in the case of no coupling with passive element ($d_2=0$). Hence the introduction of a passive element may lead to both a decrease and increase in the synchronization threshold due to a decrease or increase in the effective frequency mismatch between the oscillatory elements, respectively. Notice that when the influence of the passive element is too large ($d_2\gtrsim 0.28$) then the effect of oscillation death takes place.

Figure 4(b) illustrates the dependency of the synchronization frequency ω_s on the parameter d_2. Comparing this curve with the ones in Fig. 2, one can state that the synchronization frequency increases with growth of d_2 for almost the same values of d_2 when the frequency of the single element increases with enlarging the coupling to the passive element and vice versa. In other words, the character of the curve in Fig. 4(b) is defined mainly by the kind of dependency of the frequency of the single oscillatory element on the coupling with the passive element (Fig. 2). The analytical description of these effects is given in Sec. II C.

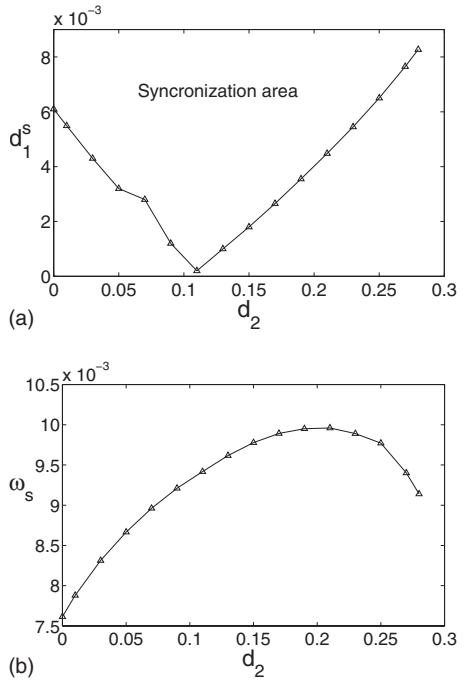

FIG. 4. Influence of a passive element on the synchronization properties of two coupled Bonhoeffer–Van der Pol oscillators: (a) dependency of the synchronization threshold d_1^s on coupling with a passive element d_2; (b) dependency of the synchronization frequency on the coupling parameter d_2.

C. Analytical description based on the model of coupled phase oscillators

In this section the analytical description of the effects described above is given. According to the Malkin's theorem [17], a phase model of a chain of locally and weakly coupled nonidentical periodic oscillators can be generally written as

$$\dot{\phi}_j = \omega_j + \varepsilon h(\phi_{j-1} - \phi_j) + \varepsilon h(\phi_{j+1} - \phi_j), \tag{7}$$

where $j=1,\ldots,N$, N is the number of oscillators, ω_j are the individual frequencies, ε characterizes coupling, and h is a 2π-periodic coupling function. In our case, numerical experiments demonstrated that it is possible to choose the h function as a sinus in the first approximation. Let us consider the system of two coupled periodic oscillators with different individual frequencies. According to Eq. (7) the phase dynamics of the system can be written as follows:

$$\dot{\varphi}_1 = \omega_1(d_2) + d_1 \sin(\varphi_2 - \varphi_1),$$

$$\dot{\varphi}_2 = \omega_2(d_2) + d_1 \sin(\varphi_1 - \varphi_2). \tag{8}$$

Here the term including coefficient d_1 describes the coupling between oscillatory elements while the influence of the passive element on this system is represented by two dependencies of frequencies of phase oscillators $\omega_1(d_2)$ and $\omega_2(d_2)$ on some parameter d_2 that characterizes the degree of the passive element impact. In case of $d_1=0$ and $d_2=0$, the system (8) describes two oscillatory elements with different individual frequencies $\omega_1(0)$ and $\omega_2(0)$. For dependencies $\omega_1(d_2)$ and $\omega_2(d_2)$, we use the polynomial approximations of analogous curves obtained for the Bonhoeffer–Van der Pol model (Fig. 2) for the parameter values $a_o=0.3$ and $a_o=0.25$. An approximation of these curves using a third order polynomial gives

$$\omega_1(d_2) = -0.13d_2^3 - 0.024d_2^2 + 0.02d_2 + 0.007\,7,$$

$$\omega_2(d_2) = 0.021d_2^3 - 0.079d_2^2 + 0.028d_2 + 0.007\,3. \tag{9}$$

Let us come now from the system (8) to the equation for phase differences,

$$\dot{\phi} = \omega_2(d_2) - \omega_1(d_2) - 2d_1 \sin(\phi), \tag{10}$$

where $\phi=\varphi_2-\varphi_1$. The criterion of synchronization in this case involves the existence and stability of a steady state,

$$\bar{\phi} = \arcsin\frac{\omega_2(d_2) - \omega_1(d_2)}{2}, \tag{11}$$

for system (10) that is ensured by the fulfillment of the inequality,

$$d_1 > \frac{\omega_2(d_2) - \omega_1(d_2)}{2}. \tag{12}$$

It is easy to show also that the synchronization frequency ω_s in this case is defined by the equation,

$$\omega_s = \frac{\omega_2(d_2) + \omega_1(d_2)}{2}. \tag{13}$$

Analytical curves for the synchronization threshold $d_1(d_2)$ and the synchronization frequency $\omega_s(d_2)$ obtained according to the Eqs. (12) and (13) are shown in Figs. 5(a) and 5(b), respectively.

These curves very well match the results of the numerical simulations with a Bonhoeffer–Van der Pol model and may—in an analytical way—support the claim that the introduction of a passive element can lead to a decrease or increase in the synchronization threshold.

III. SYNCHRONIZATION OF CARDIOMYOCYTES UNDER THE FIBROBLASTS IMPACT

In the current section and in Secs. III–V, we present results obtained using the model of cardiac cell dynamics. In Sec. I it has already been noticed that the heart consists of cells of different types. Among them one can single out oscillatory cardiac cells (pacemakers) and passive cardiac cells (fibroblasts). Further, for convenience in description, the biological terms pacemaker (fibroblast) and nonlinear dynamics oscillatory (passive) cell are considered as synonyms.

A. Cardiac cells models

In the numerical experiments, biologically relevant models describing electrical activity of cardiac cells were used. As a model of oscillatory cardiac cell (pacemaker), we use the Luo-Rudy phase 1 model [18]. This is the Hodgkin-Huxley-type model [19] consisting of eight nonlinear differ-

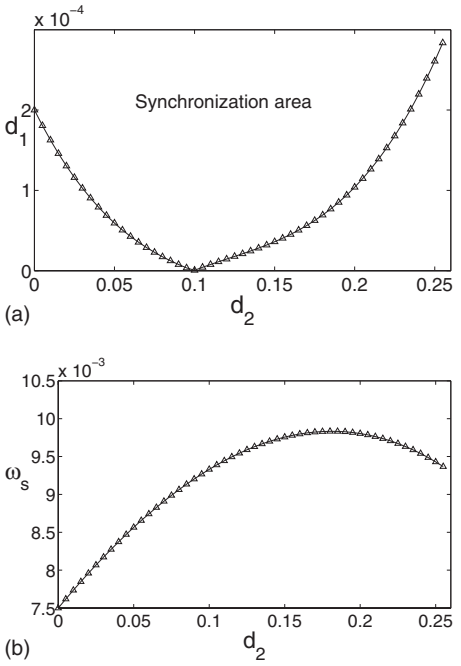

FIG. 5. Analytical curves for (a) synchronization threshold $d_1(d_2)$ and (b) synchronization frequency $\omega_s(d_2)$ obtained according to the analytical equations for the system of coupled phase oscillators.

ential equations. The first equation describes the action potential V rate of change,

$$C_m \frac{dV}{dt} = -(I_{\text{ion}} + I^{\text{ext}}), \tag{14}$$

where V denotes the cell membrane voltage measured in millivolts, $C_m = 1\ \mu\text{F/cm}^2$ is the membrane capacity. The time unit of the model is 1 ms. I^{ext} is a constant external electrical stimulus and I_{ion} is a sum of six ionic currents flowing through the membrane,

$$I_{\text{ion}} = I_{\text{Na}} + I_{si} + I_{\text{K}} + I_{\text{K1}} + I_{\text{K}p} + I_b, \tag{15}$$

where I_{Na} is a sodium current, I_{si} is the slow inward calcium current, I_{K} is potassium current, I_{K1} is stationary potassium current, $I_{\text{K}p}$ is plateau potassium current, and I_b is a background current. These currents are measured in $\mu\text{A/cm}^2$ and defined by

$$I_{\text{Na}} = G_{\text{Na}} m^3 hj(V - E_{\text{Na}}),$$

$$I_{si} = G_{si} df[V - E_{si}(V,c)],$$

$$I_{\text{K}} = G_{\text{K}} x x_i(V)(V - E_{\text{K}}),$$

$$I_{\text{K}_1} = G_{\text{K1}} k_{1i}(V)(V - E_{\text{K1}}),$$

$$I_{\text{K}_p} = G_{\text{K}p} k_p(V)(V - E_{\text{K1}}),$$

$$I_B = G_b(V - E_b). \tag{16}$$

Here G_q and E_q for $q \in \{\text{Na}, si, \text{K}, \text{K1}, \text{K}p, b\}$ denote, respectively, the maximal conductance and the reversal potential of the corresponding ionic current. Each of the gating variables $g_i \in \{m,h,j,d,f,x\}$, $i = 1,\ldots,6$ is described by the ordinary differential equation as follows:

$$\dot{g}_i = \alpha_{g_i}(V)(1 - g_i) - \beta_{g_i}(V) g_i. \tag{17}$$

Nonlinear functions $\alpha_{g_i}(V)$ and $\beta_{g_i}(V)$ as well as $E_{si}(V,c)$, $x_i(V)$, $\text{K}_{1i}(V)$, and $\text{K}_p(V)$ are fitted to the experimental data [18]. The dynamics of the external concentration of calcium ions is given by the first-order differential equation,

$$\dot{c} = 10^{-4} I_{si}(V,d,f,c) + 0.07(10^{-4} - c). \tag{18}$$

In this system, we emphasize two control parameters: I^{ext} and G_{K1}. The variation of these parameters allows to change the dynamics of the isolated Luo-Rudy element from the excitable regime to the oscillatory and vice versa. There are two ways to obtain self-oscillations in the system using these control parameters.

(i) For the standard value of parameter $G_{\text{K1}} = 0.604\ 7$, the value of parameter I^{ext} is varied. The parameters G_{K} and G_{si} in this case are also different from their original values and equal to 0.705 and 0.07, respectively. It is done in order to approximate the action potential duration (APD) generated by such a system to the APD of the human heart [20]. Further we will call such a system an oscillatory Luo-Rudy element of the first type.

(ii) For the standard value of parameter $I^{\text{ext}} = 0$, the value of parameter G_{K1} is varied [21]. In the sequel, we will call such a system an oscillatory Luo-Rudy element of the second type.

These two types of oscillatory Luo-Rudy elements demonstrate different bifurcations leading to transition from excitable to oscillatory regime and vice versa. It is shown further in the paper that these differences between the two types of oscillatory Luo-Rudy elements play an important role in the interaction of them with passive elements.

As a model of fibroblast, we use the Kohl [22] model of a passive cardiac cell. This system is described by the simple first-order linear differential equation,

$$\dot{V}_F = -\frac{1}{C_F} G_F(V_F - E^{\text{rest}}). \tag{19}$$

The key parameter here is E^{rest} which is the resting potential of fibroblast that may vary in the range from −60 to −10 mV. In the second part of the paper, it is demonstrated that fibroblasts with different values of E^{rest} influence the wave dynamics of coupled oscillatory cardiac cells in different ways.

Let us now briefly discuss the bifurcations that lead to the change in the dynamical behavior in the Luo-Rudy oscillatory elements of the first and the second types from excitable to oscillatory and vice versa. Figure 6(a) illustrates the dependency of the oscillation amplitude A of the first type Luo-Rudy element on the parameter I^{ext} for the isolated element and for the element under the influence of fibroblast with $E^{\text{rest}} = -40$ and −20 mV. When $I^{\text{ext}} = 0$ the element is in excitable regime. For the value $I^{\text{ext}} \approx -2.21$, in the phase space of the system a stable limit cycle occurs via the saddle-node bifurcation on invariant curve and the element starts to dem-

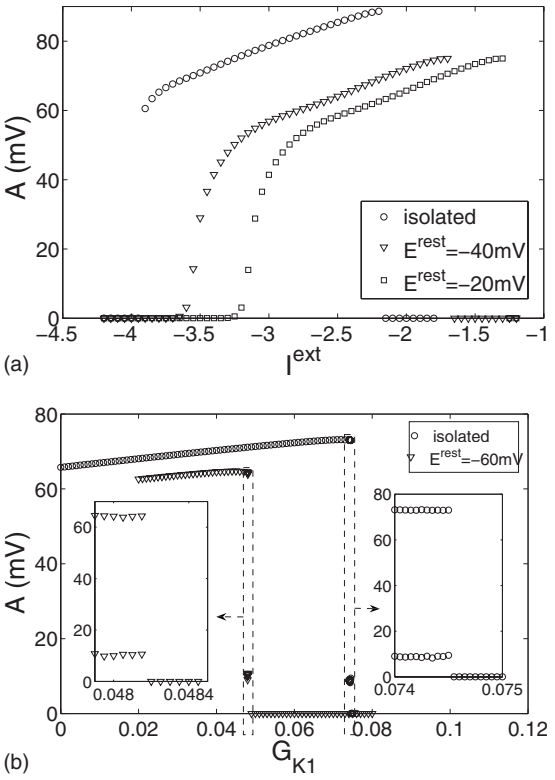

FIG. 6. Dependency of the oscillation amplitude A (a) of the first type Luo-Rudy element on the parameter I^{ext} for the isolated element and for the element under the influence of fibroblast with $E^{\text{rest}}=-40$ and -20 mV; (b) of the second type Luo-Rudy element on the parameter G_{K1} for the isolated element and for the element under the influence of fibroblast with $E^{\text{rest}}=-60$ mV.

onstrate periodic behavior. A further decrease of I^{ext} up to -4 leads to a reduction in the oscillation amplitude A. For $I^{\text{ext}} \approx -4.04$ the stable limit cycle corresponding to the self-oscillations in the element disappears due to saddle-node limit cycle bifurcation. Thus, the element comes back again to the excitable regime [16]. Introduction of fibroblasts in this system affects only the second bifurcation that provides the disappearance of the stable limit cycle. The analysis of the matrix eigenvalues of the linearization in the steady state proves that in this case it is caused by a supercritical Andronov-Hopf bifurcation accompanied with merging of the stable limit cycle into the steady state [Fig. 6(a)].

In Fig. 6(b) the dependency of the oscillation amplitude A of the second type Luo-Rudy element on the parameter I^{ext} is presented for the isolated element and for the element under the influence of fibroblast with $E^{\text{rest}}=-60$ mV. For physically relevant values of the parameter $G_{\text{K1}}>0$, one can observe here a transition from oscillatory to excitable regime when $G_{\text{K1}} \approx 0.08$ for the isolated element. Let us consider a little more detailed the bifurcation that provides this effect. It was ascertained that in the system having initially the only steady state of a saddle type, the saddle-node bifurcation takes place for $G_{\text{K1}}=0.06$. As a result, two more steady states appear. With a further increase in control parameter up to $G_{\text{K1}}=0.074$, one of the steady states acquires stability via an Andronov-Hopf bifurcation that is proved by the analysis of the roots of the corresponding characteristic equation. This

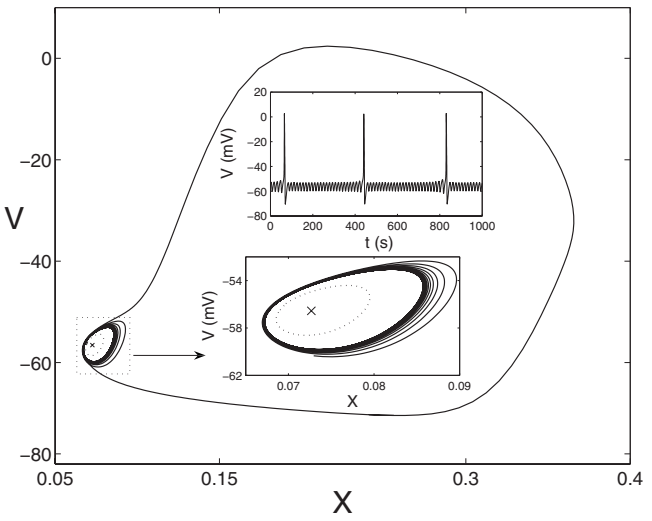

FIG. 7. The projection of stable and unstable limit cycles as well as stable steady state into the coordinate plane (V,X) for $G_{\text{K1}}=0.074\,5$. The time series corresponding to the stable limit cycle is presented in the upper inset.

bifurcation is subcritical and it is accompanied with the birth of an unstable limit cycle. This fact is indicated by the existence of bistability in the system, i.e., coexistence of a stable limit cycle with a stable steady state in the phase space. Figure 7 shows the projection of stable and unstable limit cycles as well as stable steady state into the coordinate plane (V,X) for $G_{\text{K1}}=0.074\,5$. Then the stable and unstable limit cycles merge and disappear via a saddle-node limit cycle bifurcation for $G_{\text{K1}}=0.074\,52$. Notice that beforehand the stable limit cycle is changing its form, as shown in Fig. 7. In particular one can observe subthreshold oscillations of low amplitude. The time series corresponding to that stable limit cycle is presented in the upper inset in Fig. 7. The parameter range of G_{K1}, when such subthreshold oscillations are observed, may be estimated by the insets in Fig. 6(b). Here the small values of amplitude A correspond to low amplitude subthreshold oscillations.

B. Fibroblast impact on the oscillatory cardiac cell dynamics

As demonstrated in Secs. II A and II B using the Bonhoeffer–Van der Pol model, it is possible to judge qualitatively the influence of a passive element on the synchronization properties in oscillatory ensembles from the character of the dependency of the single oscillatory element frequency on the coupling with a passive element (Fig. 2). So, in order to understand if it is possible to obtain effects such as those that were observed in Secs. II A and II B, but in the case of coupled cardiac cells, the dependencies of frequency of single pacemaker on the coupling with fibroblast d were obtained. Figures 8(a) and 8(b) show the curves for the oscillatory Luo-Rudy element of the first type under the unidirectional fibroblast influence with $E^{\text{rest}}=-60$ mV (a) and $E^{\text{rest}}=-20$ mV (b) for different values of parameter I^{ext}, i.e., for different individual frequencies of pacemaker. It is clearly seen that introduction of fibroblast with any resting potential within the range $E^{\text{rest}} \in [-60,-20]$ mV leads to a

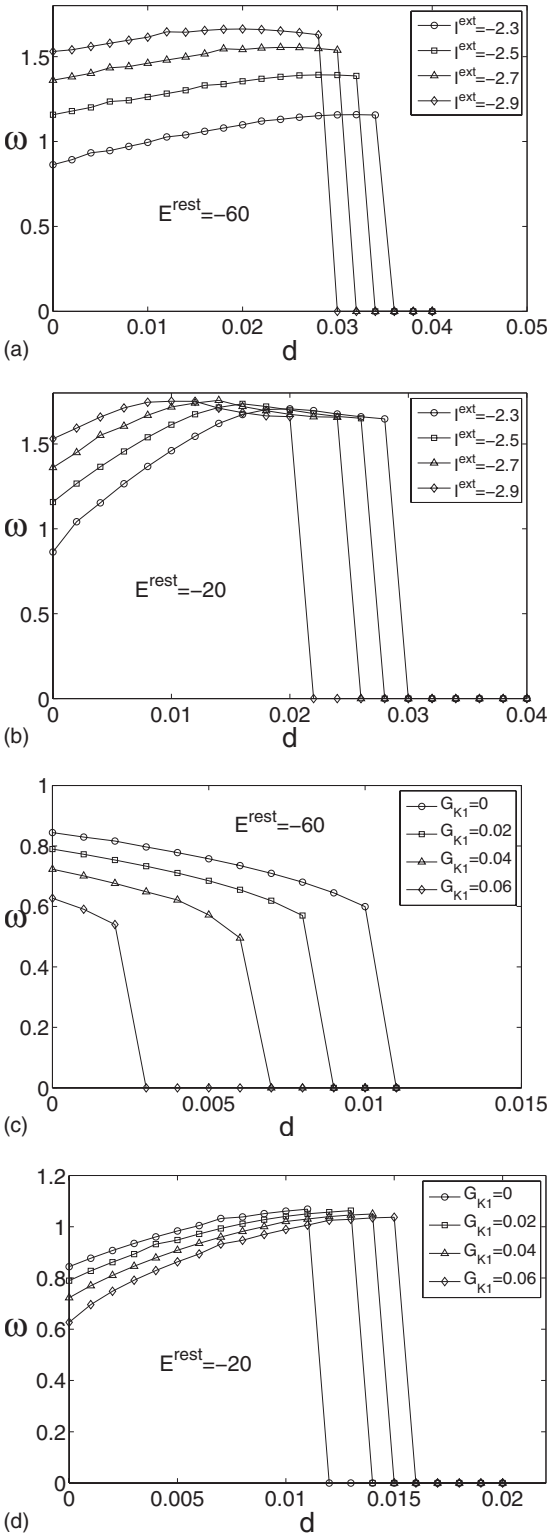

FIG. 8. The curves of dependency of the single pacemaker frequency on the coupling with fibroblast: [(a) and (b)] the curves for oscillatory Luo-Rudy element of the first type for different values of parameter I^{ext} and resting potential of fibroblast (a) $E^{\text{rest}}=-60$ mV and (b) $E^{\text{rest}}=-20$ mV; [(c) and (d)] the curves for oscillatory Luo-Rudy element of the second type for different values of parameter G_{K1} and resting potential of fibroblast (c) $E^{\text{rest}}=-60$ mV and (d) $E^{\text{rest}}=-20$ mV.

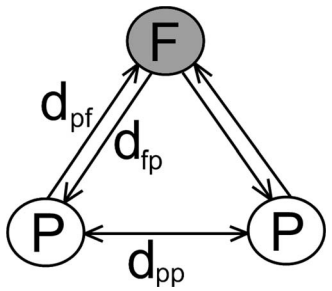

FIG. 9. The topology of the investigated system of three elements. Pacemakers are presented with white color and letter "P." The fibroblast is presented with gray color and letter "F." The parameters d_{pp}, d_{fp}, d_{pf} are the coefficients of diffusive coupling between elements.

decrease in the effective frequency mismatch and increase in the pacemaker frequency. The value of E^{rest} in this case affects just the degree of the effects development.

Another situation is observed for the oscillatory Luo-Rudy element of the second type. Analogous frequency dependencies are presented in Figs. 8(c) and 8(d). One can observe here that the influence of fibroblast with $E^{\text{rest}}=-20$ mV results in a decrease in the effective frequency mismatch as well as a significant increase in the oscillation frequency [Fig. 8(d)], while the impact of passive element with $E^{\text{rest}}=-60$ mV appears to be right opposite [Fig. 8(c)]. It is also worth noticing that there is such a threshold value of $E^{\text{rest}}\approx-45$ mV when no significant change of neither the frequency mismatch nor the pacemaker oscillation frequency can be observed. The last important point here is that in all considered cases there exists some critical value of the coupling with fibroblast starting from which the oscillations in the systems vanish. In other words the effect of oscillatory death [16] takes place here like it was also observed with Bonhoeffer–Van der Pol elements.

Thus, analyzing the dependencies in Fig. 8 one can suppose that it is possible to obtain synchronization of two different oscillatory cardiac cells due to the fibroblast impact. In the case of oscillatory Luo-Rudy element of the first type, it is possible for any values (from the range observed) of fibroblast resting potential. For the second type Luo-Rudy element, it is only possible for $E^{\text{rest}}\gtrsim-45$ mV. The numerical simulations results confirming this fact are presented in Sec. III C.

C. Synchronization of two pacemakers due to the fibroblast

In this section, the results of numerical simulations of the system of three coupled elements (Fig. 9) are presented. Let us consider two coupled pacemakers (in Fig. 9 they are presented with white color and letter "P") under the fibroblast influence (in Fig. 9 it is presented with gray color and letter "F"). Let us also consider three new parameters d_{pp}, d_{fp}, d_{pf} denoting, respectively, (i) symmetrical diffusive coupling between oscillatory elements, (ii) the coupling directed from fibroblast to pacemakers, and (iii) the coupling directed from pacemaker to fibroblast.

Figures 10(a) and 10(b) show the dependency of frequencies of two pacemakers on coupling with fibroblast d_{fp} for

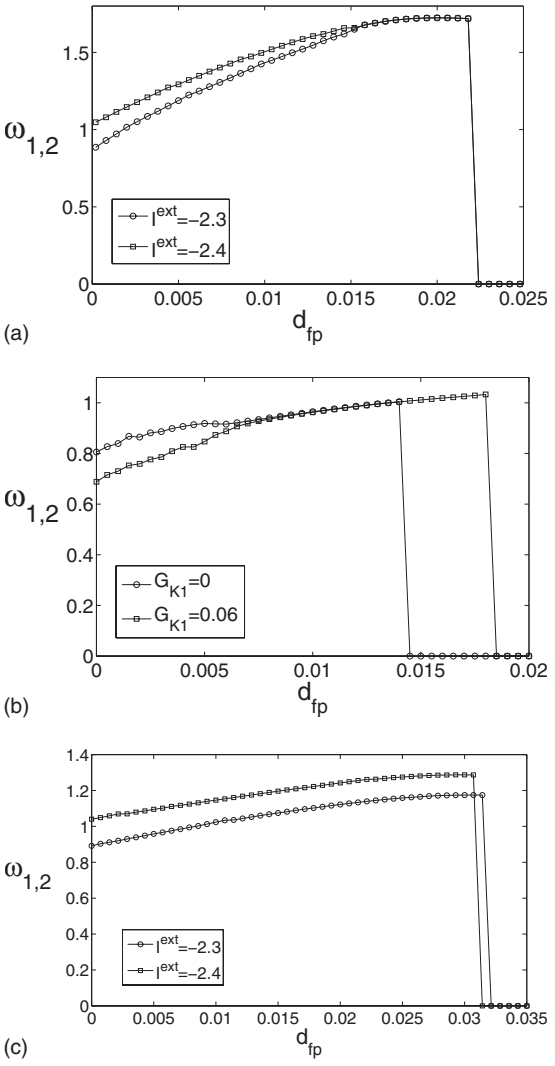

FIG. 10. The dependency of frequencies of two pacemakers on the coupling with fibroblast d_{fp} for the cases when the pacemakers are (a) oscillatory Luo-Rudy elements of the first type and (b) oscillatory Luo-Rudy elements of the second type. In both cases, the fibroblast resting potential is $E^{\text{rest}}=-30$ mV. One can observe that the synchronization sets in with increase of d_{fp}. (c) The dependency of frequencies of two pacemakers on the coupling with fibroblast d_{fp} for oscillatory Luo-Rudy elements of the first type and for fibroblast resting potential $E^{\text{rest}}=-60$ mV. No synchronization can be observed here.

the cases when the pacemakers are oscillatory Luo-Rudy elements of the first [Fig. 10(a)] and second [Fig. 10(b)] types. In both cases, the resting potential of fibroblast E^{rest} was equal to −30 mV and coupling parameters are (a) $d_{pp}=0.000\,5$, $d_{pf}=0$; (b) $d_{pp}=0.001$, $d_{pf}=0$. Hence, we deal with the limit case of the unidirectional coupling. The control parameters defining individual frequencies are (a) $I_1^{\text{ext}}=-2.3$, $I_2^{\text{ext}}=-2.4$; (b) $G_{\text{K1}}^1=0$; $G_{\text{K1}}^2=0.06$. It is seen from Fig. 10 that the increase in coupling from fibroblasts leads to the convergence of individual pacemakers frequencies and for the chosen parameters in both cases the regime of synchronization of two pacemakers sets in starting from some critical value d_{fp}. With further increase of d_{fp}, the effect of oscillation death also takes place. Apart from it, Fig. 10(c)

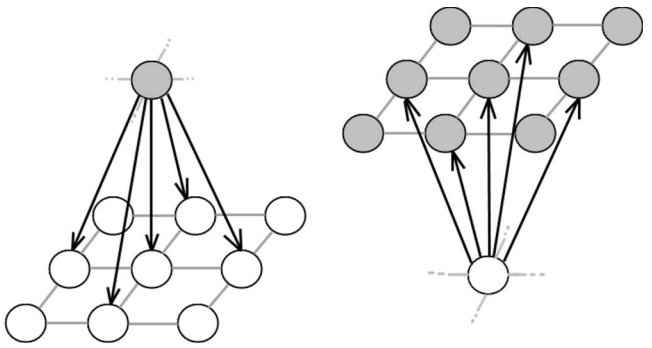

FIG. 11. The topology of the studied system: two two-dimensional lattices of 200×200 elements located one above the other. White colored circles denote pacemakers; gray colored circles denote fibroblasts.

shows the same dependency as one in Fig. 10(a) but for the value of fibroblast resting potential $E^{\text{rest}}=-60$ mV. In this case the regime of synchronization between pacemakers cannot be achieved because the influence of fibroblast with $E^{\text{rest}}=-60$ mV does not provide convergence of individual frequencies of pacemakers. This fact confirms that the steady state of passive element (resting potential of fibroblast) is an important parameter defining whether it is possible to obtain synchronization or not. Thus, the results of numerical simulations support the preliminary qualitative analysis given in Sec. III B.

D. Synchronization in large oscillatory ensembles

As far as many real systems are distributed ensembles of a large number of coupled elements, in order to demonstrate the generality of the effects obtained earlier, we performed a set of numerical experiments with the systems composed of a large number of oscillators. The concrete topology of the studied system is shown in Fig. 11.

This topology is two two-dimensional lattices of 200×200 elements located one above the other. The lower lattice consists of oscillatory Luo-Rudy elements of the first type with a random distribution for the control parameter $I_i^{\text{ext}}\in[-2.4,-2.3]$ defining individual frequencies of pacemakers. The upper lattice is composed of identical fibroblasts with resting potential $E^{\text{rest}}=-40$ mV. The coupling between the elements of each lattice is the diffusive coupling with four nearest neighbors. The coupling between lattices is organized in such a way that each element of one lattice is coupled with five nearest elements of the other lattice (Fig. 11). The boundary conditions in each lattice are zero flux. This topology is an approximation to the real sinoatrial node consisting of mixed oscillatory and passive cells. Like it was done earlier in Sec. III C, let us introduce coupling coefficients $d_{pp}=0.000\,1$, $d_{pf}=0$. The coefficient d_{fp} is varied. Let us also introduce a new coefficient $d_{ff}=0.3$ describing the coupling strength between fibroblasts in the upper lattice. In the numerical experiments, for each value of parameter d_{fp}, the average oscillation frequencies of all oscillatory elements of the lower lattice were calculated.

The results of these calculations are presented in Fig. 12. Here the ordinate axis shows the frequencies of each oscil-

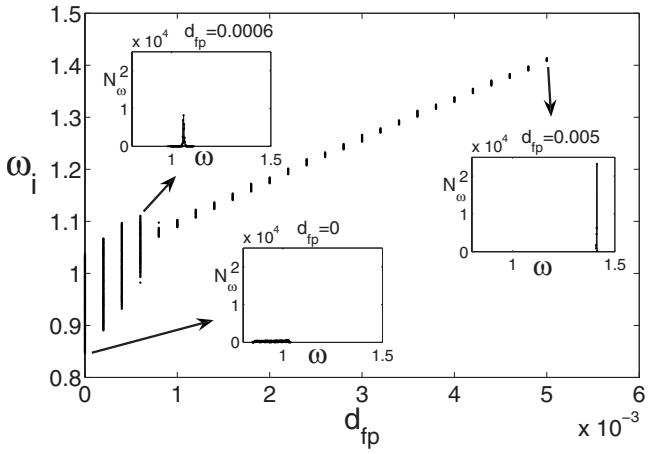

FIG. 12. Dependency of the frequency of every oscillatory element in the lower lattice on coupling with fibroblasts d_{fp}. Three insets present distributions of the number of oscillatory elements on frequencies $N_\omega(\omega)$ for three fixed values $d_{fp} \in \{0, 0.000\,6, 0.005\}$. One can observe that synchronization sets in with increase of d_{fp}.

latory element in the lower lattice and abscissa axis shows the coupling of these elements with fibroblasts d_{fp}. The three insets in Fig. 12 illustrate the frequency distribution of the number of oscillatory elements $N_\omega(\omega)$ for three fixed values $d_{fp} \in \{0; 0.000\,6; 0.005\}$. In other words $N_\omega(\omega^*)$ is the number of pacemakers oscillating with the frequency ω^*. It is seen from the figure that initially for $d_{fp}=0$ the oscillation frequencies in the lower lattice are distributed randomly and uniformly in the range from 0.85 to 1.03 Hz (see corresponding inset in Fig. 12). This indicates that there is no synchronization in the system. With the increase in fibroblast impact d_{fp}, the range of the observed frequencies significantly narrows and for $d_{fp}=0.000\,6$ is about [0.99,1.11] Hz. At the same time, the significant peak appears in the distribution N_ω (inset $d_{fp}=0.000\,6$ in Fig. 12). Thus more elements become to oscillate with the same frequency indicating that synchronization starts to set in. Finally, for high enough values of d_{fp}, the regime of complete synchronization takes place in the system. So, for example, for $d_{fp}=0.005$ one can see that the distribution N_ω is nothing but narrow and highly peaked, corresponding to a synchronization regime. Notice that with the increase in the impact from fibroblasts on pacemakers, the average frequency of oscillations also increases as it was in the experiments in Sec. III C. Apart from it, like in Secs. III A–III C, the effect of oscillatory death can also be observed here starting from the value $d \approx 0.005$. Thus, in this section we demonstrated the possibility of the synchronization regime onset in the large oscillatory ensemble due to the coupling of oscillatory elements with passive ones.

In order to compare the obtained results with real biological experiments one may turn, for example, to the paper [16]. There the results of real biological experiments with cardiac cells cultures composed of pacemakers and fibroblasts are presented. It is shown in [16] that with the increase in coupling of pacemakers with fibroblasts in the culture of oscillatory cardiac cells, the regime of synchronization sets in; moreover it is accompanied with the growth of the average oscillation frequency in the system. Thus, the results obtained in numerical and analytical studies find their confirmation in nature.

IV. INFLUENCE OF PASSIVE ELEMENTS ON THE WAVE DYNAMICS OF OSCILLATORY ENSEMBLES

In this section we present the investigation results of passive elements influence on characteristics of wave dynamics of oscillatory ensembles such as (i) conduction velocity, (ii) frequency, and (iii) amplitude. All the results are discussed in the context of cardiac cultures dynamics. However, they can be generalized to the case of interaction of any oscillatory and passive elements. This part of the paper consists of three sections: (i) in Sec. IV A we give the motivation of this research and motivation of selection of the models for numerical experiments, (ii) in Sec. IV B the results of the study of one-dimensional ensembles are presented, and (iii) in Sec. IV C these results are extended and generalized for two-dimensional systems.

A. Biological experiments: Problem statement

As a problem statement and a motivation of our following research, we use the results of real biological experiments performed with the cultures of cardiac cells and presented in [23]. In this work, the influence of fibroblasts on such characteristics of collective dynamics of oscillatory cardiac cells as conduction velocity, frequency, and amplitude of oscillations is observed. During the experiments, it was discovered that an increase in the number of fibroblasts in the system leads to the (i) decrease in action potential wave propagation velocity (i.e., increase in propagation delay), (ii) decrease in amplitude of the wave, and (iii) decrease in the average oscillation frequency of pacemakers. The last result allows us to define which model to use in numerical experiments. As the model of oscillatory Luo-Rudy element of the first type under the influence of fibroblast with any resting potential E^{rest} demonstrates the increase in the average oscillation frequency of single element then it cannot be used to describe effects presented in [23]. On the contrary for the oscillatory Luo-Rudy element of the second type, one can observe both an increase and decrease in the oscillation frequency of pacemaker interacting with fibroblast in dependency on the resting potential. That is why this system was chosen for simulations. It is also worth saying that the results presented in [23] differ from the data described in [16]. There is a supposition that these differences take place because of using of fibroblast with different values of E^{rest}. In Sec. IV B the results of fibroblasts influence on the wave dynamics in one-dimensional oscillatory ensemble are presented.

B. Influence of fibroblasts on the wave dynamics of oscillatory elements: One-dimensional case

In this section, we present the results of study of the fibroblast influence on the wave propagation delay T_d which is inverse proportion to wave conductance velocity, wave amplitude A, and average oscillation frequency Ω in a one-dimensional oscillatory ensemble of coupled cardiac cells, i.e., in a chain of pacemakers. The structure of the system in

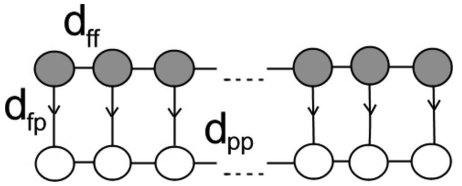

FIG. 13. Topology of the studied system: two one-dimensional chains of 100 elements located parallel to each other. White colored circles denote pacemakers; gray colored circles denote fibroblasts.

question is shown in Fig. 13. This system consists of two one-dimensional chains of 100 elements located parallel to each other. One chain consists of Luo-Rudy elements of the second type with the parameter G_{K1} (that defines individual frequencies of pacemakers) distributed in such a way that for the fixed value of coupling parameter $d_{pp}=0.02$ and no coupling with fibroblasts in this chain, the regime of global synchronization sets in corresponding to the impulse propagating along the structure from the first element to the last one. In particular, $G^i_{\mathrm{K1}}=G^1_{\mathrm{K1}}+i\Delta$, $i=\overline{1,N}$, where $G^1_{\mathrm{K1}}=0$, $\Delta=0.000\,6$. The second chain is composed of identical fibroblast with resting potential E^{rest} which is being chosen different from one experiment to another. The coupling coefficient between fibroblasts d_{ff} in every case equals 0.1.

The purpose of these experiments was to obtain the dependencies of various wave processes characteristics (T_d, A, Ω) in the system on coupling parameter d_{fp} and in this case the coupling was unidirectional at that, i.e., $d_{pf}=0$. It is worth reminding that in biological experiments [23], these characteristics were investigated depending on the number of fibroblasts. Nevertheless, in the case of identical passive cells and unidirectional coupling from fibroblasts to pacemakers, the variation in the whole number of fibroblasts is equivalent to the variation of parameter d_{fp}. In the limit cases $d_{fp}=0$ or $d_{fp}=1$, there are no fibroblasts in the system or their number equals the number of pacemakers, respectively.

Figure 14(a) demonstrates the dependency of wave propagation delay T_d on coupling with fibroblasts d_{fp} for different values of resting potential E^{rest}. One can see that for the values of E^{rest} equal to −60 and −50 mV the delay time T_d significantly increases with growth of d_{fp}. So, for example, for $E^{\mathrm{rest}}=-60$ mV the delay for $d_{fp}=0.011$ is increased by about 83% in comparison to the initial value for $d_{fp}=0$. For much higher fibroblast resting potentials −20 and −10 mV the opposite situation is observed. For $E^{\mathrm{rest}}=-20$ mV, for example, the delay T_d decreases from 4200 to 2100 ms while d_{fp} increases from 0 to 0.009. For the intermediate values of E^{rest} (e.g., 30 mV), the value of propagation delay almost does not change.

Within the bounds of the stated problem other characteristics of collective dynamics of the system in question were also considered. Figure 14 also illustrates the dependencies of the synchronization frequency in the chain Ω [Fig. 14(b)] and wave amplitude A [Fig. 14(c)] on the parameter d_{fp}. It is seen from Fig. 14(c) that with the increase in fibroblast influence on pacemakers, the amplitude A decreases regardless of the value of the resting potential E^{rest} of the passive elements. This can be explained as follows. The growth of d_{fp}

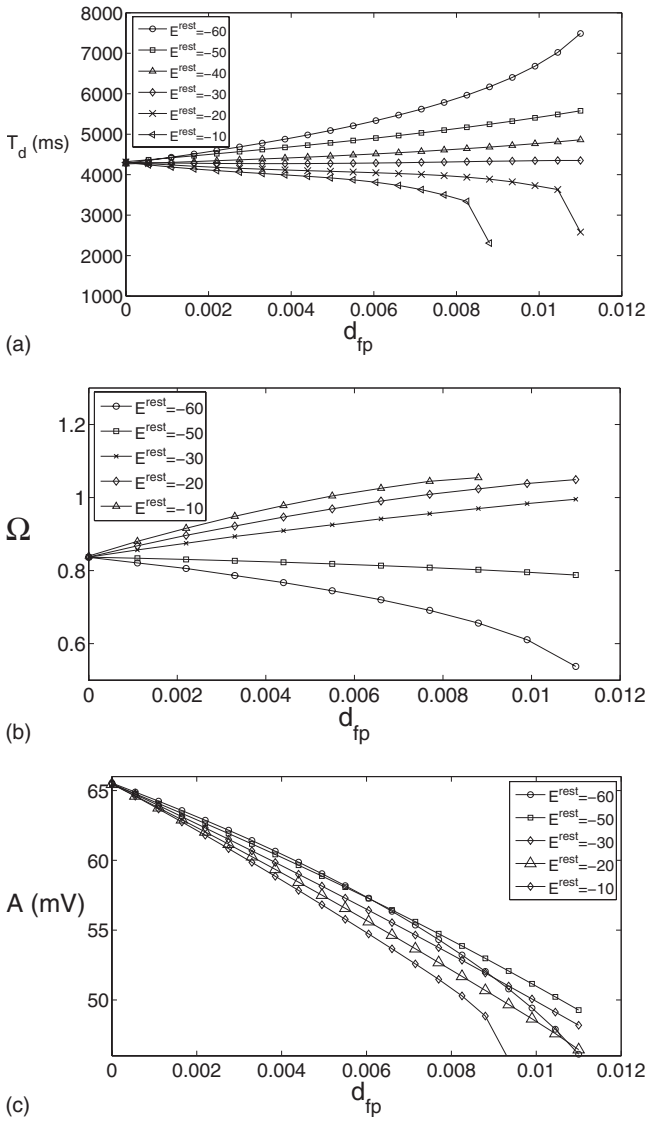

FIG. 14. (a) The dependency of wave propagation delay T_d on coupling with fibroblasts d_{fp} for different values of the resting potential E^{rest}. For $E^{\mathrm{rest}}=-60$ and −50 mV, one can observe a significant increase in wave propagation delay while for $E^{\mathrm{rest}}=-10$ and −20 mV the delay appreciably decreases. For the intermediate values of $E^{\mathrm{rest}}=-30$ mV the influence of fibroblasts on conduction velocity seems not to be significant. The dependencies of (b) the synchronization frequency in the chain Ω and (c) the wave amplitude A on the coupling with fibroblasts d_{fp} for different values of the resting potential E^{rest}. For $E^{\mathrm{rest}}=-6$ and −50 mV the synchronization frequency in the chain decreases with growth of d_{fp} while for $E^{\mathrm{rest}}=-10$, −20, and −30 mV Ω significantly increases. In all cases, the wave amplitude significantly decreases with growth of d_{fp}.

brings the system closer to the supercritical Andronov-Hopf bifurcation accompanied with the merging of the stable limit cycle into the steady state and eventually leading to the occurrence of the oscillatory death effect. One can see from Fig. 14(b) that the synchronization frequency of the chain depending on coupling parameter d_{fp} behaves differently for different E^{rest}. So, for $E^{\mathrm{rest}}=-30$, −20, and −10 mV Ω significantly increases with growth of d_{fp} while for $E^{\mathrm{rest}}=-60$

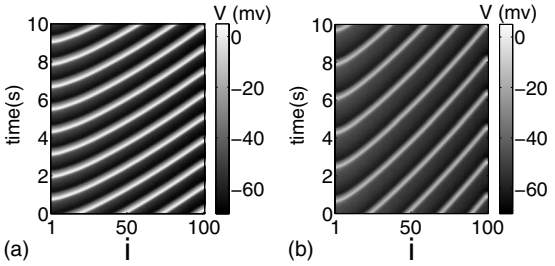

FIG. 15. Spatiotemporal diagrams of the processes for $E^{\text{rest}}=-60$ mV and for coupling values (a) $d_{fp}=0$ and (b) $d_{fp}=0.011$. The increase in the propagation delay T_d, the decrease in the synchronization frequency, and the decrease in the wave amplitude with growth of d_{fp} is observed.

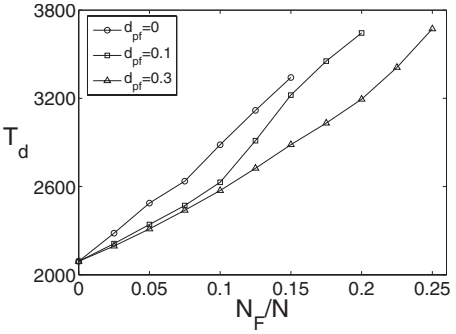

FIG. 16. The dependencies of the delay T_d of concentric wave propagation in the lattice on the number of fibroblasts N_F to the whole number of elements in the system N for different values of the coupling from pacemakers to fibroblasts $d_{pf} \in \{0, 0.1, 0.3\}$.

and −50 mV the synchronization frequency decreases. The qualitative explanation of this effect is that for single Luo-Rudy element of the second type being under the fibroblast impact, the oscillation frequency (i) increases for $E^{\text{rest}} \gtrsim -40$ mV and (ii) decreases for $E^{\text{rest}} \lesssim -40$ mV [16].

For more clearness in Figs. 15(a) and 15(b) two spatiotemporal diagrams of the processes are presented for $E^{\text{rest}}=-60$ mV and for values of the coupling $d_{fp} \in \{0, 0.011\}$, respectively. In these diagrams, the color corresponds to the value of oscillatory elements voltage, the slope of propagating wave fronts illustrates the delay T_d, and the time period of two consequent wave fronts characterizes the oscillation period, i.e., this time period is in inverse proportion to the synchronization frequency. Comparing these two diagrams with each other, one can clearly see (i) the increase in the wave propagation delay T_d, (ii) the increase in the pulse repetition period, i.e., the decrease in the synchronization frequency, and (iii) the decrease in the wave amplitude with growth of d_{fp}.

In order to explain qualitatively the observed effect, let us compare the obtained results with the dependencies of frequencies of a single oscillatory Luo-Rudy element of the second type being under the impact of fibroblast, which are presented in Figs. 8(a) and 8(b) in Sec. III B. As it was discussed earlier, the influence of fibroblast with the resting potential $E^{\text{rest}}=-60$ mV leads to an increase in the effective frequency mismatch between pacemakers [Fig. 8(a)] while the impact of a passive element with $E^{\text{rest}}=-20$ diminishes this mismatch [Fig. 8(b)]. Comparing Figs. 14, 8(a), and 8(b) one can make an assumption that a decrease or increase in the effective frequency mismatch between the elements of the chain of oscillatory cardiac cells due to the fibroblasts impact leads, respectively, to the an increase or decrease in the wave propagation delay T_d in this system.

Thus, analyzing the obtained results one can conclude that in cases $E^{\text{rest}}=-60$ and −50 mV the observed system demonstrates a qualitative agreement with data of biological experiments. Particularly, in this system, such as in the real experiments, one can observe (i) an increase in wave-front propagation delay, (ii) the decrease in the synchronization frequency, and (iii) the decrease in the wave amplitude with the growing influence from the fibroblasts to the oscillatory cardiac cells ensemble.

C. Two-dimensional case

In Sec. IV B we considered the influence of fibroblasts on oscillatory cardiac ensembles in the one-dimensional case. However, for generality and completeness of the paper, the two-dimensional case of the same problem should also be considered because this is a more adequate approach with respect to the real experiments [23] where cardiac cells cultures placed into the Petri dish are two-dimensional structures. Let us consider a two-dimensional lattice of 100×100 elements composed of passive cells and oscillatory Luo-Rudy elements of the second type with a random distribution of the parameter G_{K1} in the range [0.04, 0.06]. Besides, in one corner of the lattice we organized an area of 10×10 elements with $G_{\text{K1}}=0$, i.e., the elements with individual frequencies being higher than all the other individual frequencies in the system. It was done in order to obtain a regime of global synchronization in the lattice presented with a concentric wave propagating from the corner. In this case, it is easy to calculate the delays of wave propagation in the system. The introduction of passive elements is equivalent to the random replacement of oscillatory cells of the lattice by fibroblasts with $E^{\text{rest}}=-60$ mV except 100 special cells (discussed above) in the corner providing synchronization in the system. In this case, the wave propagation delays are calculated for a different percentage of fibroblasts in the lattice and for fixed coupling parameters $d_{pp}=0.2$, $d_{ff}=0.1$ and $d_{fp}=0.008$, $d_{pf}=0$. The case $d_{pf}=0$ is the limit case of unidirectional coupling from fibroblasts to pacemakers and it does not correspond to the real situation. Therefore the cases $d_{pf}=0.1, 0.3$ were observed as well.

Figure 16 shows the dependencies of the delay T_d of concentric wave propagation from the one corner of the lattice to the opposite one on the relation of the number of fibroblasts in the lattice N_F to the whole number of elements in the system N for different values of the coupling from pacemakers to fibroblasts $d_{pf} \in \{0, 0.1, 0.3\}$. One can clearly see that in all observed cases the increasing number of passive elements in the lattice leads to the increase in the wave propagation delay that is in agreement with the results presented earlier. Apart from it, the introduction of the inverse influence from pacemakers to fibroblasts ($d_{pf} > 0$) diminishes the impact of the passive elements, namely, for $d_{pf}=0.1, 0.3$ the

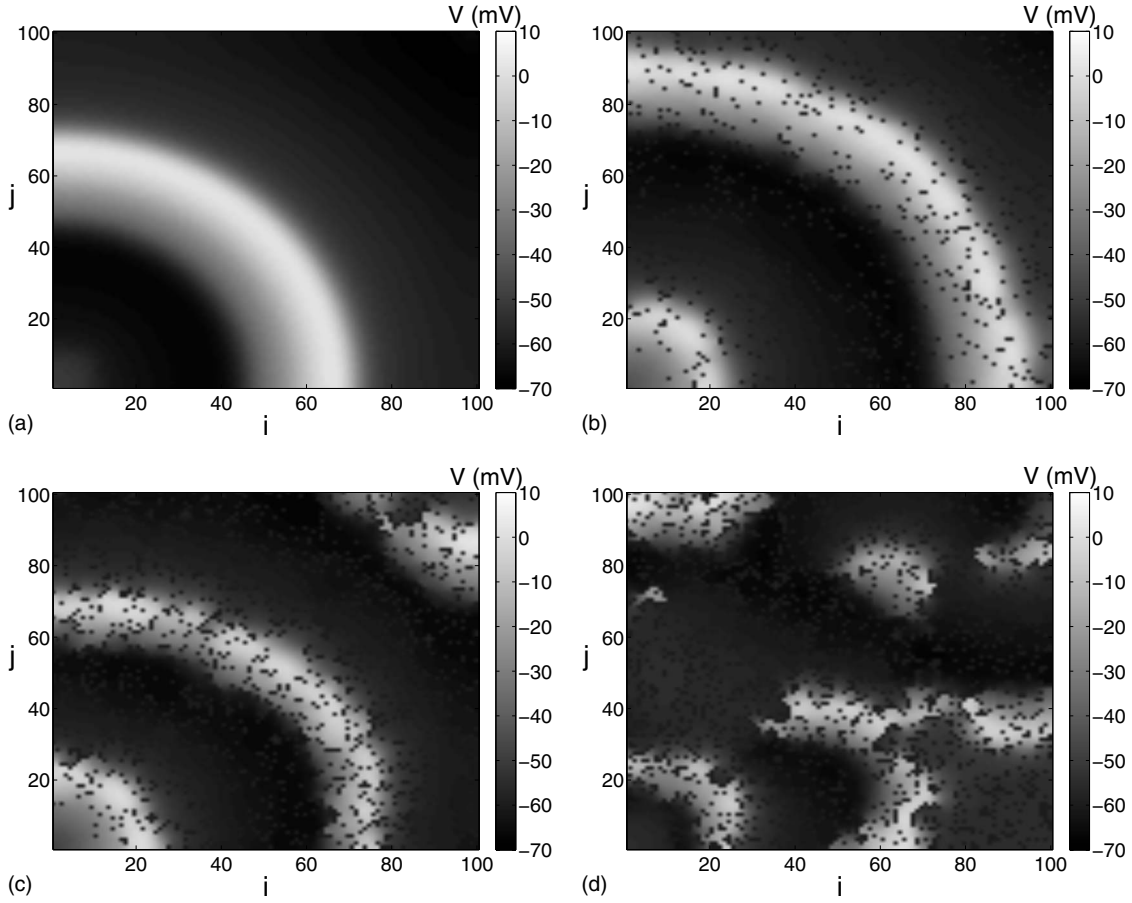

FIG. 17. Voltage snapshots of the lattice in the case of $d_{pf}=0$ for four values of $N_F/N \in 0, 0.075, 0.15, 0.2$.

slope of the curves in Fig. 16 is less than for $d_{pf}=0$. In other words, for every d_{fp} the delay T_d in these cases is less than for $d_{pf}=0$.

It is also worth noticing that all the curves in Fig. 16 are bounded from the right by some critical value of N_F/N. Starting form this value, the inhomogeneity in the system defined by fibroblasts becomes large enough for the concentric wave propagating from the corner of the lattice to break up into spiral waves. In that case, there is no point of speaking about propagation delays. Figure 17 illustrates the snapshots of voltage of the lattice in case of $d_{pf}=0$ for four values $N_F/N \in \{0, 0.075, 0.15, 0.2\}$.

The figure shows that an initially smooth concentric wave front becomes more inhomogeneous [12] with the increase in fibroblasts number [Figs. 17(a)–17(c)] and completely brakes up into spiral waves for $N_F/N=0.2$ [Fig. 17(d)]. In this case the areas of fibroblasts in the lattice form the obstacles large enough to make the concentric wave front to collapse. Thus, the results of numerical experiments with two-dimensional systems demonstrate a good agreement with the data of biological research as well as with analytical estimations.

V. CONCLUSIONS

In this paper the influence of passive elements on the collective dynamics of oscillatory ensembles was considered. The emphasis is put on two major effects: (i) the influence of passive elements on the synchronization properties of ensembles of coupled nonidentical oscillatory elements and (ii) the influence of passive elements on the wave dynamics of such systems.

With the use of numerical experiments as well as analytical results, it was shown that the introduction of passive elements may lead to both an increase and decrease in the effective frequency mismatch between oscillatory elements. It was also demonstrated that in order to predict qualitatively the possibility of this effect occurrence, one can turn to the dependency of single oscillatory element frequency on coupling with the passive element. If, for example, these dependencies for different individual frequencies of oscillatory element have an intersection point then it is possible to obtain the synchronization threshold to be equal zero tuning the coupling with passive element.

The second part of the paper dealt with the influence of passive elements on the wave dynamics of oscillatory elements, namely, (i) wave conduction velocity, (ii) wave amplitude, and (iii) synchronization frequency. It was obtained that the key parameter defining the character of passive element's impact in this case is the steady state of this passive element or, speaking in terms of cardiac dynamics modeling, the resting potential of fibroblast E^{rest}. For small values of E^{rest}, for example −60 mV, it was shown that the wave conduction velocity as well as the synchronization frequency

decrease with the increase of passive elements impact. For the high values of the resting potential, for example, −20 mV, the completely opposite situation is observed. Besides, in every observed case the introduction of passive elements leads to the decrease in the oscillation amplitude in the system and eventually to the oscillation death effect occurrence. The results obtained in this paper were compared with the data of real biological experiments and demonstrate a good agreement with them.

ACKNOWLEDGMENTS

This work is done at financial support of RFBR under Projects No. 06-02-16596, No. 08-02-97049, and No. 08-02-92004. J.A.S. acknowledges support from K. U. Leuven, the Flemish government, FWO, and the Belgian federal science policy office (Grants No. FWO G.0226.06, No. CoE EF/05/006, GOA AMBioRICS, IUAP DYSCO, and No. BIL/05/43).

[1] H. Haken, *Advanced Synergetics* (Springer-Verlag, Berlin, 1983).
[2] Y. Kuramoto, *Chemical Oscillations and Turbulence* (Springer, Tokyo, 1984).
[3] A. T. Winfree, *The Geometry of Biological Time* (Springer, New York, 1980).
[4] P. A. Tass, *Phase resetting in medicine and biology* (Springer, Berlin, 1999).
[5] G. Bub, A. Shrier, and L. Glass, Phys. Rev. Lett. **88**, 058101 (2002).
[6] G. Bub, A. Shrier, and L. Glass, Phys. Rev. Lett. **94**, 028105 (2005).
[7] B. Blasius and R. Tönjes, Phys. Rev. Lett. **95**, 084101 (2005).
[8] J. H. E. Cartwright, Phys. Rev. E **62**, 1149 (2000).
[9] J. Kurths, N. Wessel, R. Bauernschmitt, and W. Ditto, Chaos **17**, 015101 (2007).
[10] D. Noble, Chaos, Solitons Fractals **5**, 321 (1995).
[11] I. Shiraishi, T. Takamatsu, T. Mimikawa, Z. Onouchi, and S. Fujita, Circulation **85**, 2176 (1992).
[12] K. H. W. J. Ten Tusscher and A. V. Panfilov, Europace **9**, vi38 (2007).
[13] M. Miragoli, N. Salvarini, and S. Rohr, Circ. Res. **101**, 755 (2007).
[14] V. Jacquemet, Phys. Rev. E **74**, 011908 (2006).
[15] D. Pazó and E. Montbrió, Phys. Rev. E **73**, 055202(R) (2006).
[16] A. K. Kryukov, V. S. Petrov, L. S. Averyanova, G. V. Osipov, W. Chen, O. Drugova, and C. K. Chan, Chaos **18**, 037129 (2008).
[17] F. C. Hoppensteadt and E. M. Izhikevich, *Weakly Connected Neural Networks* (Springer-Verlag, Berlin, 1997).
[18] C.-H. Luo and Y. Rudy, Circ. Res. **68**, 1501 (1991).
[19] A. L. Hodgkin and A. F. Huxley, J. Physiol. (London) **117**, 500 (1952).
[20] Z. Qu, J. N. Weiss, and A. Garfinkel, J. Physiol. London **276**, 269 (1999).
[21] W. C. Tong and A. V. Holden, *Induced Pacemaker Activity in virtual Mannalian Ventricular Cells* (Springer-Verlag, Berlin, 2005), Vol. 226.
[22] P. Kohl, A. G. Kamkin, I. S. Kiseleva, and D. Noble, Exp. Physiol. **79**, 943 (1994).
[23] J. P. Fahrenbach, R. Mejia-Alvarez, and K. Banach, J. Physiol. London **585**, 565 (2007).